ACS OMEGA

http://pubs.acs.org/journal/acsodf

Article

Molecular Modeling of Pentacyclic Aromatic Bislactam-Based Small Donor Molecules by Altering Auxiliary End-Capped Acceptors to Elevate the Photovoltaic Attributes of Organic Solar Cells

Mahnoor Qaisar, Saba Zahid, Rasheed Ahmad Khera,* Yaser A. El-Badry, Muhammad Umar Saeed, Rana Farhat Mehmood, and Javed Iqbal*

Cite This: *ACS Omega* 2022, 7, 20528−20541

Read Online

ACCESS | Metrics & More | Article Recommendations | Supporting Information

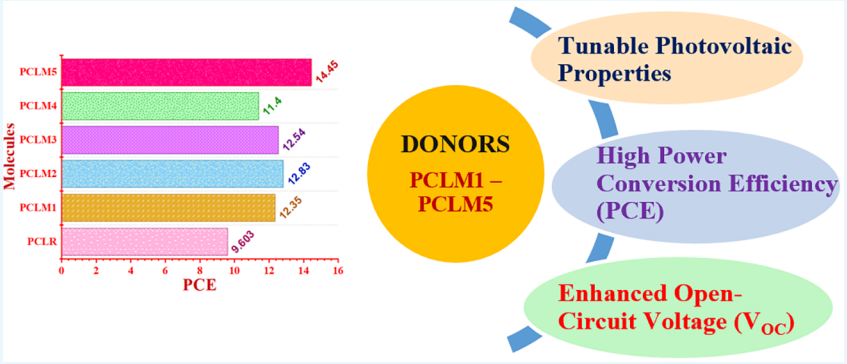

ABSTRACT: Small-molecule (SM)-based organic solar cells (OSCs) have dominated the photovoltaic industry on account of their efficient optical and electronic properties. This quantum mechanical study addresses a DFT study of pentacyclic aromatic bislactam (PCL)-based small molecules for extremely proficient OSCs. Five novel small molecules (**PCLM1−PCLM5**) retaining the A−π−A−π−D−π−A−π−A arrangement were fabricated from the reference **PCLR**. At the MPW1PW91/6-31G** level of theory, detailed profiling of these novel molecules was performed by accurately following DFT, along with the time-dependent density functional theory (TD-DFT) hypothetical simulations to analyze the UV−visible absorption (λ_{max}), light-harvesting efficiency (LHE), dipole moment (μ), fill factor (FF), open-circuit voltage (V_{OC}), power conversion efficiency (PCE), frontier molecular orbitals (FMOs), binding energy (E_b), density of states (DOS), electrostatic potential (ESP), and transition density matrix (TDM) plots. Alteration of peripheral acceptors in all of the molecular structures drastically modified their charge-transfer properties, such as a strong light-harvesting capability in the range of 0.9993−0.9998, reduced exciton E_b (from 0.34 to 0.39 eV), a reduced bandgap (E_g) in the range of 1.66−1.99 eV, an elevated λ_{max} (775−959 nm) along with a higher μ in the solvent phase (1.934−7.865 D) when studied in comparison with **PCLR**, possessing an LHE of 0.9986, an E_b of 0.40, an E_g 2.27 eV, λ_{max} at 662 nm, and a μ of 0.628 D. The FMO analysis revealed the uniform dispersal of charge density entirely along the highest occupied (HOMO) and lowest unoccupied (LUMO) molecular orbitals in newly constructed moieties. Electron as well as hole mobility rates, V_{OC}, FF, and PCE of all novel molecules (**PCLM1−PCLM5**) were higher as compared with those of **PCLR**, ultimately making them exceptional candidates for solar devices. Focusing on the outcomes, terminal acceptor modification was found to be a suitable method for the development of highly tuned OSCs in the future.

1. INTRODUCTION

The exhaustion of nonrenewable natural energy resources such as coal, oil, natural gas, and nuclear energy has drastic effects on the natural environment. Besides, these resources also present a risk to human beings as they cause environmental pollution.[1] To overcome the ongoing energy crisis, substitute renewable energy supplies such as biomass, hydropower plants, solar energy, etc., are being utilized. Solar energy supply is the most significant and limitless form of energy that can satisfy the energy demands of mankind. The use of photovoltaic cells, which directly convert solar energy into electrical power, is one of the best ways to harness solar energy currently. Earlier, inorganic silicon-based solar cells (SCs) were used owing to their elevated power conversion efficiency (PCE).[2] Despite this, inorganic SCs have

Received: January 1, 2022
Accepted: May 19, 2022
Published: June 8, 2022

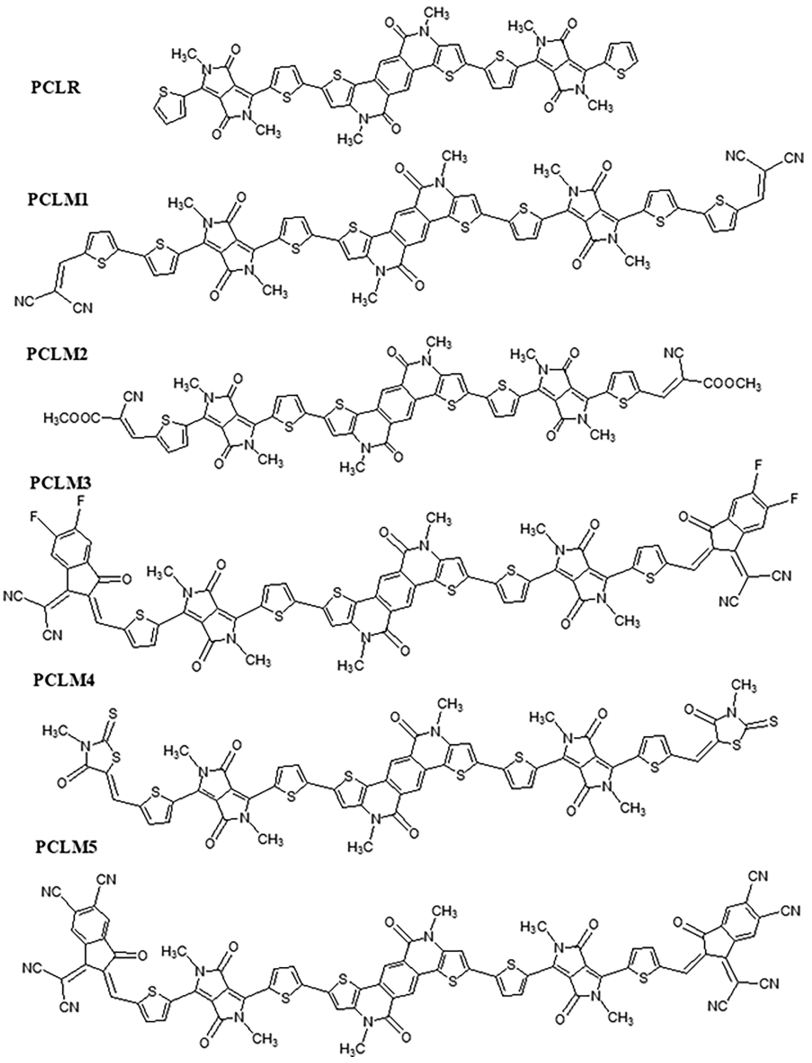

Figure 1. ChemDraw sketches of **PCLR** and **PCLM1**−**PCLM5**.

major drawbacks, including their high cost, rigidity, susceptibility to heat changes, and inability to adjust the energy level.[3] These negative features of silicon-based inorganic SCs have given rise to a persistent desire to find suitable alternatives.

Organic solar cells (OSCs) have gained considerable attention recently for converting solar power into electricity owing to their properties of light weight, flexibility, ease of fabrication, and cost-efficient production processes.[4] When it comes to portable devices, OSCs have provided new possibilities.[5] The development of the bulk heterojunction OSCs caused to an improvement in the efficiency of SCs made from organic materials.[6] Because of their elevated photoabsorption coefficient, enhanced stability, and robustness, OSCs may have an enhanced PCE when associated with silicon-based SCs.[7] There are several organic molecules that may be altered to construct novel and enhanced photovoltaic materials.[8]

Over the past few decades, the operating efficiency of fullerene OSCs has increased by 11.7%. Simultaneously, non-fullerene-based organic photovoltaic cells (NF-OPVs) have made significant development due to their tunable energy levels, specific absorption spectra, and electron mobilities.[9] These attributes are absent in fullerene derivatives due to their limited chemical modification. The low voltage loss and tunable optoelectronic features of NF-OPVs, together with their synthetic flexibility and broad spectral range, make them easy to adapt architecturally to satisfy the project's objectives while also allowing PCEs of over 17%.[10]

Several molecular modeling approaches such as alkyl chain substitution, interfacial alterations of donor−acceptor units, and alteration of end-capped terminal moieties have been exploited to further increase the energy efficiency of NF systems.[11] Recently, novel organic materials such as pentacyclic aromatic bislactam,[12] benzodifurandione-based poly(phenylene vinylene) (BDPPV),[13] and diketopyrrolopyrrole (DPP) acceptors[14] have been explored as promising building blocks for OPVs. DPP exhibits a range of desirable optical characteristics and adequate solubility in organic solvents. The DPP unit is a rigid and planar aromatic structure that improves the intermolecular packing in molecules and offers higher charge mobilities.[15]

In the current project, five novel molecules (**PCLM1**−**PCLM5**) were designed from the reference molecule named **PCLR. PCLR** possesses two monomers, an electron-deficient pentacyclic aromatic bislactam (PCL) central core followed by thiophene rings attached on both sides of PCL, which are further preceded by DPP and a thiophene ring.[16] The technique of structural modification was used to design five new small donor groups from the reference **PCLR**. The five newly designed molecules were modeled by adding end-capped acceptors such

https://doi.org/10.1021/acsomega.2c00001
ACS Omega 2022, 7, 20528−20541

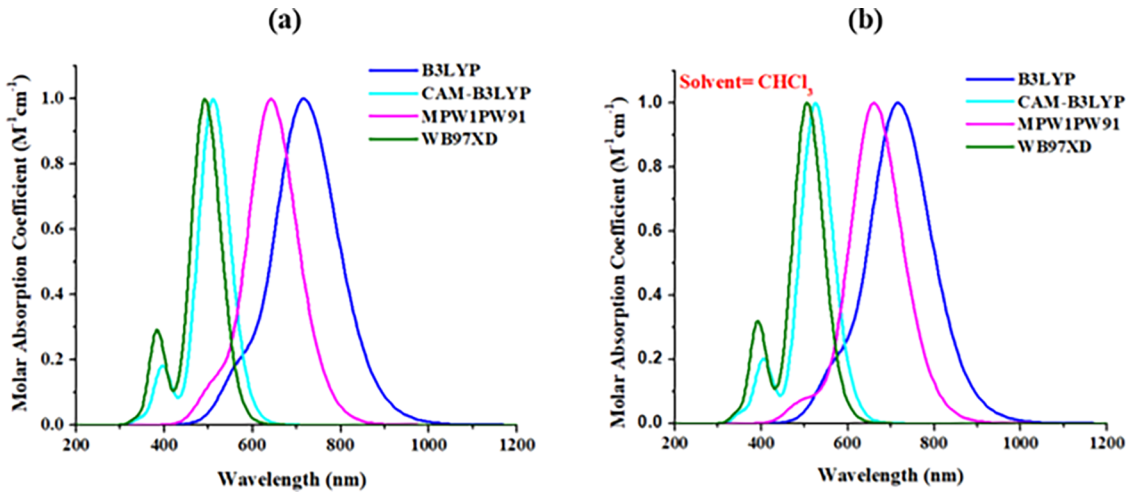

Figure 2. UV−vis absorption spectra of **PCLR** with four discrete functionals in the (a) gaseous and (b) $CHCl_3$ solvent phases.

as **X1** (2-thiophen-2-ylmethylene-malononitrile) in **PCLM1**, **X2** (2-cyano-acrylic acid methyl ester) in **PCLM2, X3** (2-(5,6-difluoro-2-methylene-3-oxo-indan-1,1-dicarbonitrile)) in **PCLM3, X4** (3-methyl-5-methylene-2-thioxo-thiazolidin-4-one) in **PCLM4**, and **X5** (2-methylene-3-oxo-indan-1,1,5,6-tetracarbonitrile) in **PCLM5** after both terminal thiophene rings (π-spacer) in the reference molecule (**PCLR**). The configuration of the reference molecule was DPP−PCL−DPP, and the five novelly designed molecules had an acceptor−DPP−PCL−DPP−acceptor configuration. ChemDraw structures of the reference (**PCLR**) and newly developed chromophores (**PCLM1−PCLM5**) are shown in Figure 1.

2. COMPUTATIONAL METHODOLOGY

The optimization, at the ground state, of the reference molecule **PCLR** was carried out with four different functionals, i.e., MPW1PW91,[17] B3LYP,[18] wB97XD,[19] and CAM-B3LYP,[20] to compare the molar absorptivity (λ_{max}) values with that of the experimental value of **PCLR**. The λ_{max} obtained with the MPW1PW91 functional for the reference **PCLR** showed good synchronization with the experimentally reported value. Further computations of newly constructed molecules were executed with MPW1PW91/6-31G**. The designed molecules **PCLM1**, **PCLM2**, **PCLM3**, **PCLM4**, and **PCLM5** were optimized by the above-stated functional and basis set. Time-dependent approach of density functional theory (TD-DFT) calculations in a gaseous medium was accomplished after structural modification to model the absorption graph of the reference **PCLR**. The influence of the solvent chloroform on IEFPCM[21] computations was also investigated. UV−visible spectra of the reference (**PCLR**) and five newly designed molecules (**PCLM1−PCLM5**) were assessed by the Swizard program.[22] Origin 6.0 software[23] was employed for the construction of the absorption graphs. To analyze the contribution of all fragments to the absorption of solar radiations, the density of states (DOS) of **PCLR** and the newly developed molecules were computed by PyMOlyze 1.1 software.[24] TDM analyses were performed using Multiwfn 3.7 software[25] to comprehend the electronic excitations with the help of the same functional selected for optimization. To calculate electron, as well as hole mobilities, of the reference **PCLR** along with the five novelly constructed molecules (**PCLM1−PCLM5**), eqs 1 and 2 based on the Marcus theory were used. The mathematical expressions of these equations are as follows:

$$\lambda_e = [E_-^0 - E_0] + [E_0^- - E_-] \quad (1)$$

$$\lambda_h = [E_+^0 - E_0] + [E_0^+ - E_+] \quad (2)$$

eq 1 expresses the electron mobility (λ_e) and eq 2 expresses the hole mobility, where E_0 is the neutral energy of the optimized molecule and E_0^- and E_0^+ are the anionic and cationic energies, respectively, at ground states computed successively from optimized neutral molecules. The cation's neutral energy is represented by E_+^0 and the anion's neutral energy is represented by E_-^0. Both were estimated using cationic and anionic optimized geometries sequentially.

3. RESULTS AND DISCUSSION

3.1. Validation of the Method and Geometric Optimization. In the current research work, the reference molecule **PCLR** was optimized with four commonly used functionals, B3LYP, MPW1PW91, wB97XD, and CAM-B3LYP, with a basis set of 6-31G (d,p). The observed absorption maxima (λ_{max}) were at 719, 663, 512, and 529 nm, respectively, in a chloroform ($CHCl_3$) solvent. Figure 2 demonstrates the absorption spectra of **PCLR** with different functionals in the gaseous (a) as well as solvent ($CHCl_3$) (b) phases.

A comparison of DFT-computed λ_{max} of **PCLR** was carried out with the experimentally reported λ_{max} of **PCLR** (675 nm). The λ_{max} displayed at the MPW1PW91 functional level with the above-stated basis set of 6-31G (d,p) (663 nm) was in agreement with experimental value (675 nm), as depicted in Figure 3 and Table 1. Therefore, all DFT calculations of the newly designed molecules (**PCLM1−PCLM5**) were executed at the MPW1PW91/6-31G** level.

The selected functional with 6-31G** was used to optimize all of the designed compounds after a scrupulous analysis. Optimized frameworks showed that all fragments of molecules arranged themselves in one plane, which facilitates efficient charge transfer. The optimized geometries of all five newly fabricated molecules (**PCLM1−PCLM5**) and the reference (**PCLR**) are displayed in Figure 4.

3.2. Frontier Molecular Orbitals (FMOs). Frontier molecular orbitals (FMOs) are important to describe the distribution of the electron cloud in the highest occupied

https://doi.org/10.1021/acsomega.2c00001
ACS Omega 2022, 7, 20528−20541

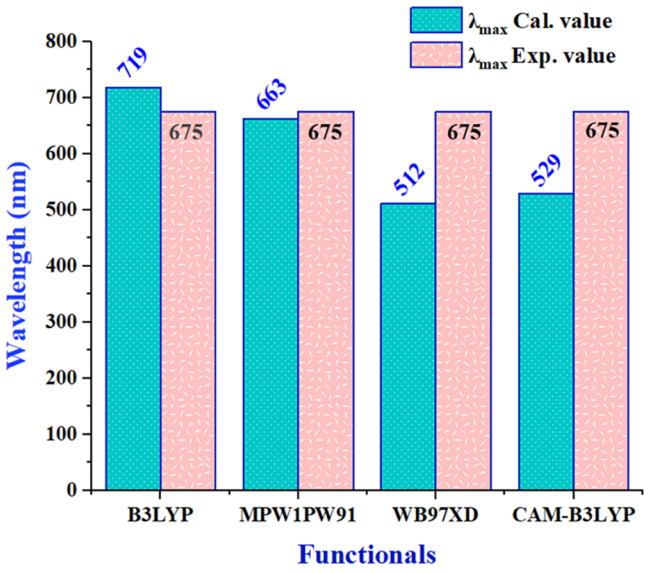

Figure 3. Bar graph of PCLR with four different functionals in the chloroform solvent with the 6-31G basis set for method validation.

Table 1. Computed λ_{max} of PCLR with Four Different Functionals

methods	λ_{max}^{cal} (nm)	λ_{max}^{exp} (nm)
B3LYP	719	675
MPW1PW91	663	
WB97XD	512	
CAM-B3LYP	529	

(HOMO) and the lowest unoccupied (LUMO) molecular orbitals. Both of these are valuable parameters to determine the efficiency of OPVs.[26,27] The intermolecular charge-transfer properties are also explored using FMOs. The thermal stability of a molecule is estimated by the bandgap (E_g) between both the FMO energy levels.[28] Charge transfer of a molecule becomes more rapid when the E_g is smaller. Hard molecules have a larger E_g, which means that they have more stability and less reactivity, whereas soft molecules have a narrow E_g as they exhibit less stability, more reactivity, and less efficient intermolecular charge-transfer attributes.[29] The newly designed chromophores (**PCLM1−PCLM5**) enhanced the charge transfer from the HOMO to the LUMO due to the presence of strong electron-withdrawing moieties and increased π-conjugation in the system. Computed HOMO/LUMO energies and E_g of the reference **PCLR** along with those of the newly designed molecules (**PCLM1−PCLM5**) with the selected functional are tabulated in Table 2.

The HOMO and LUMO values of PCLR were seen to be −5.11 and −2.84 eV, respectively, while its bandgap was 2.27 eV. All of the studied chromophores arranged in the increasing order of their HOMO energy levels were as follows: **PCLM5 > PCLM2 > PCLM3 > PCLM1 > PCLM4 > PCLR**. The trend of their LUMO values was as follows: **PCLR > PCLM3 > PCLM1 > PCLM2 = PCLM5 > PCLM4**. The HOMO and LUMO energy states of the reference **PCLR** and newly designed molecules (**PCLM1−PCLM5**) are demonstrated in Figures 5 and 6. In the present investigation, the E_g values of the reference **PCLR**, as well as the newly constructed molecules (**PCLM1−PCLM5**), were as follows: **PCLR (2.27 eV) > PCLM2 (1.99 eV) > PCLM4 (1.97 eV) > PCLM1 (1.92 eV) > PCLM3 (1.80 eV) > PCLM5 (1.66 eV)**. The E_g values of all newly designed molecules (**PCLM1−PCLM5**) were lower than that of **PCLR**. Thus, on account of their reduced E_g values, all newly developed structures were characterized as soft, polarizable, and highly reactive molecules.

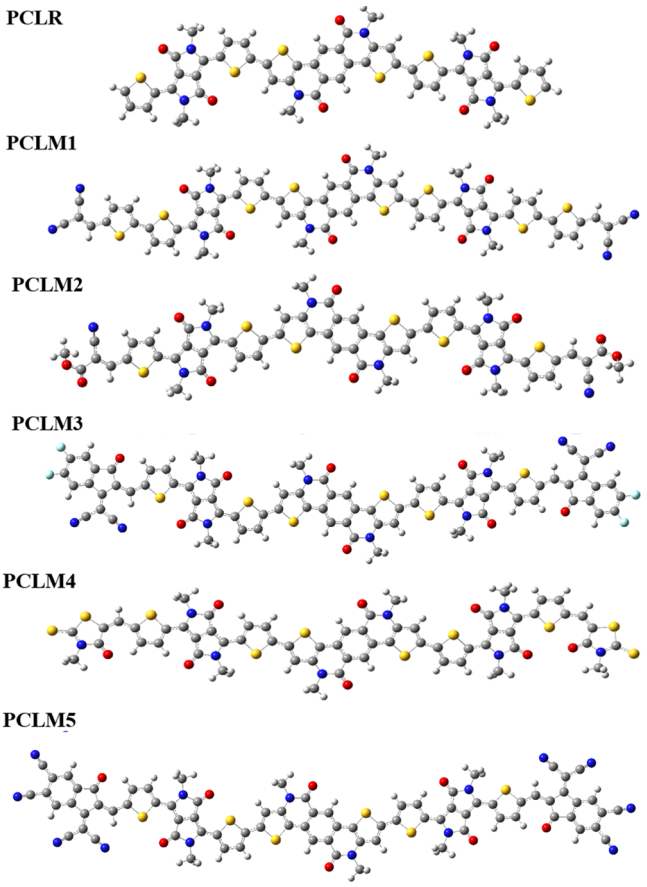

Figure 4. Ground state optimized geometries of **PCLR** along with **PCLM1−PCLM5**.

Table 2. Evaluated HOMO/LUMO Energy as well as Bandgap (E_g) values of PCLR and PCLM1−PCLM5

molecules	HOMO (eV)	LUMO (eV)	E_g (eV)
PCLR	−5.11	−2.84	2.27
PCLM1	−5.40	−3.48	1.92
PCLM2	−5.45	−3.46	1.99
PCLM3	−5.52	−3.72	1.80
PCLM4	−5.30	−3.33	1.97
PCLM5	−5.74	−4.08	1.66

The FMO plots of **PCLM1−PCLM5** showed a similar pattern of charge density in HOMOs. The charge density in HOMOs was primarily concentrated on the central donor core and π-spacers and minorly on acceptor moieties, with negligible effect on the end-capped acceptors. Similarly, the charge dispersal in LUMOs was majorly concentrated on terminal acceptor moieties and minorly on π-spacers. In case of the HOMO and LUMO of **PCLR**, the electron density was localized equally on all fragments of the molecule. FMO diagrams of all molecules are demonstrated in Figure 6.

3.3. UV−Visible Absorption Spectral Properties. Examination of UV−visible absorption features helps one to assess the working and light-harvesting efficiency of PV devices. The spectra of UV−visible absorption in all of the scrutinized

https://doi.org/10.1021/acsomega.2c00001
ACS Omega 2022, 7, 20528−20541

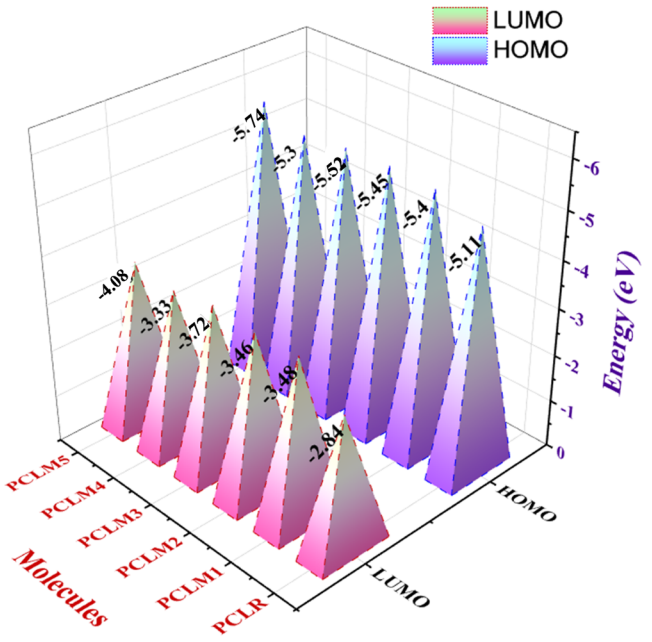

Figure 5. Representation of the highest occupied molecular orbital (HOMO) and lowest unoccupied molecular orbital (LUMO) at the elected method of DFT/MPW1PW91/6-31G (d,p), of **PCLR** and **PCLM1-−PCLM5**.

molecules with MPW1PW91/6-31G in the gaseous phase were analyzed. It was found that in comparison with **PCLR**, all newly modeled chromophores presented higher values of λ_{max}, which might be because of the influence of delocalized π-electrons on extending the conjugation with most electron-withdrawing acceptor moieties (**X1−X5**). In the meanwhile, to understand the role of the solvent on the absorption of these molecules, the λ_{max} of all molecules (**PCLM1−PCLM5**) was evaluated in chloroform ($CHCl_3$). In the presence of the $CHCl_3$ solvent, all newly designed molecules (**PCLM1−PCLM5**) along with the reference exhibited a red-shift in their absorption bands due to the stabilization of delocalized π-electrons, as shown in Figure 7. The electron-withdrawing ability of acceptor moieties is intrinsically linked to the λ_{max} and indirectly correlated to the bandgap (E_g). The reference (**PCLR**) indicated a lower λ_{max} as compared with all molecules due to the presence of the least resonance, whereas **PCLM5** acquired **X5** as an efficient electron-pulling acceptor possessing cyano groups, which resulted in its maximum absorbance. In brief, all of our designed chromophores have peripheral acceptor moieties with a strong electron-withdrawing ability.

Tables 3 and 4 display numerous photophysical properties, such as absorption maximum (λ_{max}), oscillator strength (f_{os}), excitation energy (E_x), light-harvesting energy (LHE), and the assignment of all molecules.

Excitation energy (E_x) is another crucial parameter to examine while evaluating photoelectric properties of PV devices. Low E_x values result in higher electron−hole mobilities, more efficient charge migration, and elevated power conversion efficiency (PCE). Tables 3 and 4 illustrate the values of E_x in gaseous and solvent phases. The E_x of the fabricated molecules decreases in the order of **PCLR > PCLM2 > PCLM4 > PCLM1 > PCLM3 > PCLM5** both in the gaseous and the solvent medium. All of our newly developed chromophores (**PCLM1−PCLM5**) indicated lower E_x as compared with **PCLR;** therefore, they can undergo more excitations from the ground state toward the first excited state and have a higher charge-transport potential, validating their superior photoelectronic features.

The light-harvesting efficiency (LHE) has a critical role in enhancing the efficiency of OSCs. It is important to know the LHE of molecules at a specific wavelength to determine their contribution to photon absorption. The short-circuit current is maximized when the LHE is regulated to a high value, ultimately increasing the efficiency of OSCs.[30] The LHE of the reference **PCLR** and newly designed chromophores (**PCLM1−PCLM5**) in gaseous as well as $CHCl_3$ solvent phases were estimated through eq 3, and the values are given in Tables 3 and 4.

$$\mathrm{LHE} = 1 - 10^{-f} \tag{3}$$

Here, f illustrates the oscillator strength. From the above equation, it can be observed that a higher value of oscillator strength leads to an elevated value of light-harvesting efficiency. The values of LHE computed for the reference **PCLR** and newly designed molecules (**PCLM1−PCLM5**) ranged from 0.9995 to 0.9999, as shown in Table 4. Overall, **PCLM1** had the maximum photocurrent response due to the highest LHE value of 0.9999. Graphical representations of the LHE as well as f_{oc} are illustrated in Figure 8. The LHE results indicate that the molecules newly constructed by modifying end-capped acceptors are more efficient than the reference **PCLR**.

3.4. Dipole Moment. Dipole moment (μ), a significant aspect, influences the efficiency of OPVs. The molecular solubility in solvents is estimated by the measured electronic density of an organic molecule in a given solvent. The value of μ increases with an increase in the polarity of a molecule, which improves the solubility of any molecule in the respective solvent.[31] A molecule's solubility is intimately associated with a well-ordered geometry of active layer while constructing a solar device. A smooth, thin-film morphology in OSCs leads to efficient charge transfer and enhances its efficiency.[27] Table 6 reveals the computed μ_g (gas-phase dipole moment), μ_s (solvent-phase dipole moment), and $\Delta\mu$ (difference between μ_g and μ_s) values for all of the investigated molecules.

Currently, μ lies in the range of 0.628−8.612 D in the solvent phase. Data presented in Table 5 and Figure 9 illustrate that the μ values of the newly fabricated molecules (**PCLM1−PCLM5**) are higher than that of the reference **PCLR** (**0.628**) in $CHCl_3$. Because of stronger π-interactions in $CHCl_3$ solvents, an increase in the μ value was observed for all molecules, which clarifies their higher solubility in the $CHCl_3$ solvent. **PCLM5** displayed the highest μ value due to the enhanced polarity and excellent solubility of the **X5** acceptor moiety in the $CHCl_3$ solvent. The dipole moment follows an increasing trend of **PCLR < PCLM1 < PCLM4 < PCLM2 < PCLM3 < PCLM5** both in the gaseous phase and in the chloroform solvent. Furthermore, the difference between μ_g and μ_s, i.e., $\Delta\mu$, suggests that **PCLM5** has a greater shift of μ in the $CHCl_3$ solvent. Hence the newly fabricated molecules (**PCLM1−PCLM5**) can be used as efficient molecules and solution-processable materials in designing OSCs for their strong optical results.

3.5. Density of States (DOS). In addition, the Mulliken's charge distribution through the DOS is assessed for **PCLR** and the newly constructed moieties **PCLM1−PCLM5** at the MPW1PW91/6-31G** level.[32] The DOS graphs of the newly fabricated moieties **PCLM1−PCLM5** were compared with that of the reference **PCLR** to analyze the endowment of fragments to the maximum absorption and charge density. In the DOS graphs, the negative values on the x-axis showed the HOMO energy level and positive values showed LUMO energy levels,

https://doi.org/10.1021/acsomega.2c00001
ACS Omega 2022, 7, 20528−20541

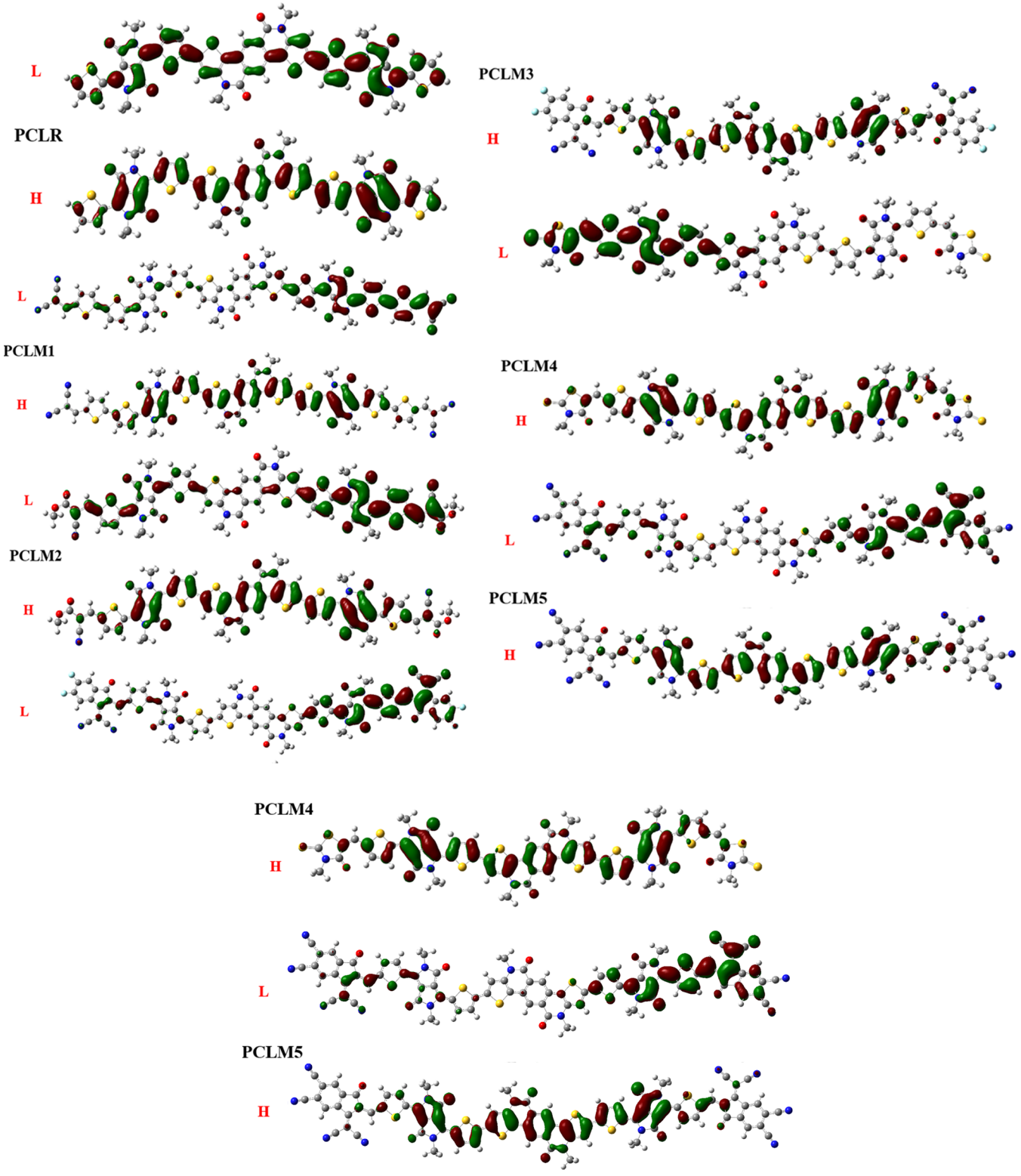

Figure 6. FMO representation of **PCLR** and **PCLM1−PCLM5**.

whereas the relative intensity of charge density was placed along the *y*-axis. For their DOS analysis, the newly fabricated chromophores (**PCLM1−PCLM5**) were allocated into three portions, namely, donors (blue), π-spacers (green), and acceptors (red). Table 6 displays the quantitative role of different fragments in forming the HOMOs and LUMOs. The density of states (DOS) graphs showed the equal and significant role of all three fragments in shifting the charge density from the HOMO to the LUMO.

The distribution pattern of all molecules is quite analogous. HOMOs are formed particularly by the contribution of spacer and acceptor fragments and slightly by the central core. The spacer made almost equal contributions to the HOMO and LUMO. Likewise, LUMOs are formed by the equal contribution

https://doi.org/10.1021/acsomega.2c00001
ACS Omega 2022, 7, 20528−20541

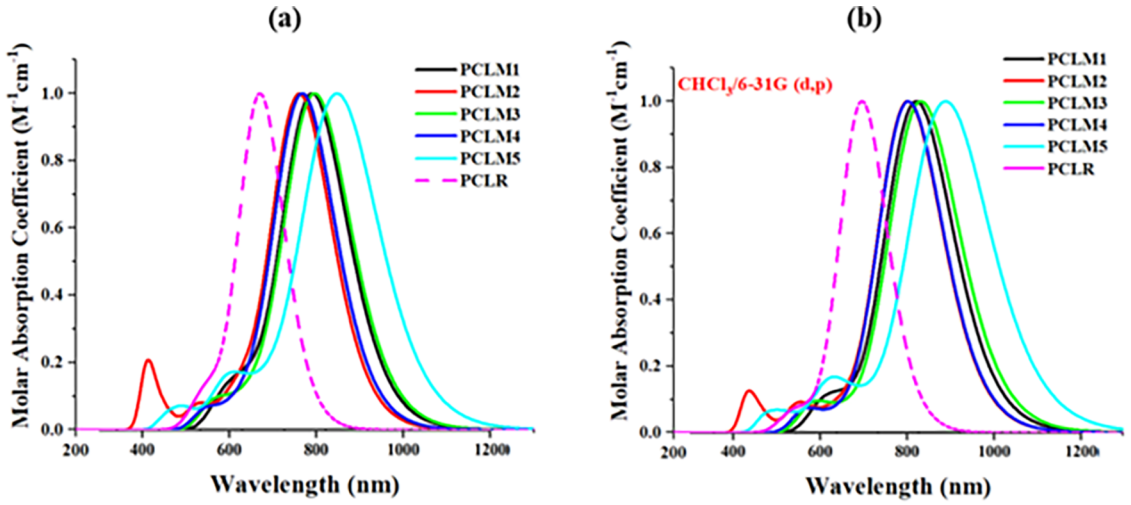

Figure 7. UV−vis spectra of **PCLR and PCLM1−PCLM5 at the** MPW1PW91/6-31G level (d,p) in the (a) gaseous and (b) solvent ($CHCl_3$) phases.

Table 3. Computed λ_{max}^{cal}, Energy of First Excitation (E_{opt}), Oscillator Strength (f_{OC}), Light-Harvesting Efficiency (LHE), along with the Major Molecular Transitions of PCLR, as well as PCLM1−PCLM5 in the Gaseous Phase

molecules	λ_{max}^{cal} (nm)	λ_{max}^{exp} (nm)	E_{opt} (eV)	f_{OC}	LHE	major molecular transitions (HOMO = H, LUMO = L)
PCLR	642	675	1.93	2.6127	0.9975	68%
PCLM1	769		1.61	3.6541	0.9998	66%
PCLM2	738		1.68	3.1634	0.9993	67%
PCLM3	824		1.50	3.4381	0.9996	65%
PCLM4	746		1.66	3.4726	0.9997	65%
PCLM5	890		1.49	3.3504	0.9995	64%

Table 4. Computed λ_{max}^{cal}, Energy of First Excitation (E_{opt}), Oscillator Strength (f_{OC}), Light-Harvesting Efficiency (LHE), as well as the Major Molecular Transitions, of PCLR along with PCLM1−PCLM5 in $CHCl_3$

molecules	λ_{max}^{cal} (nm)	λ_{max}^{exp}(nm)	E_{opt} (eV)	f_{OC}	LHE	major molecular transitions (HOMO = H, LUMO = L)
PCLR	662	675	1.87	2.8808	0.9986	68%
PCLM1	796		1.56	3.9300	0.9999	65%
PCLM2	775		1.60	3.3894	0.9995	66%
PCLM3	874		1.42	3.6540	0.9998	66%
PCLM4	777		1.59	3.7123	0.9998	65%
PCLM5	959		1.32	3.5487	0.9997	64%

of all fragments (core, spacer, and acceptor), as displayed in Figure 10.

3.6. Binding Energy (E_b) and Transition Density Matrix (TDM) Analysis. The binding energy (E_b) of excitons is another essential property for the interpretation of optical characteristics. The least amount of energy needed for the separation of excitons into free electrons and holes is defined by E_b.[33] The exciton E_b is calculated from eq 4.

$$E_b = E_{L-H} - E_x \quad (4)$$

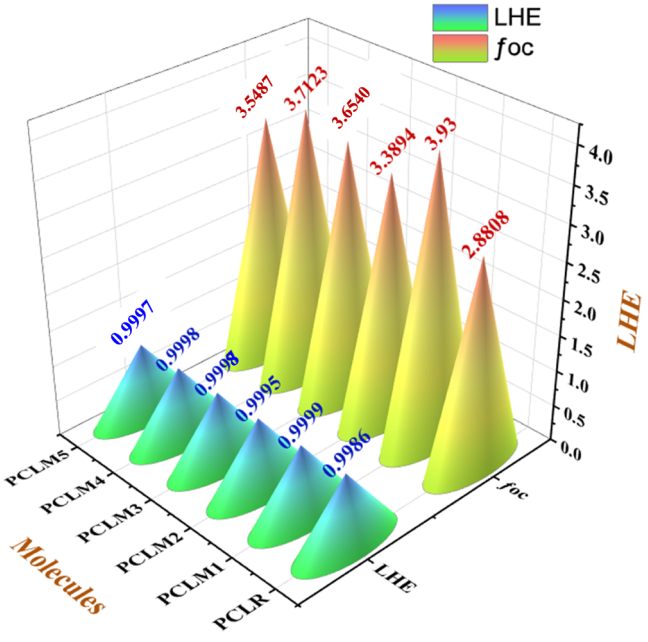

Figure 8. Oscillator strength (f_{oc}) and light-harvesting efficiency (LHE) of **PCLR** and **PCLM1−PCLM5**.

Table 5. Theoretically Computed Dipole Moments of PCLR and PCLM1−PCLM5 in the Gaseous (μ_g) and Excited (μ_s) States, along with Their Difference ($\Delta\mu$)

molecules	μ_g (D)	μ_s (D)	$\Delta\mu$ (D)
PCLR	0.619	0.628	0.009
PCLM1	1.683	1.934	0.251
PCLM2	4.530	5.368	0.838
PCLM3	5.754	6.395	0.641
PCLM4	2.563	3.340	0.777
PCLM5	6.874	7.865	0.991

where, E_b constitutes the binding energy of the exciton, E_{L-H} represents the bandgap between the evaluated FMOs, and E_x denotes the excitation energy for these FMOs.

The exciton dissociation is more advantageous if the E_b is lower, resulting in a higher current charge density.[34] Figure 11 demonstrates that all of our newly designed molecules showed

https://doi.org/10.1021/acsomega.2c00001
ACS Omega 2022, 7, 20528−20541

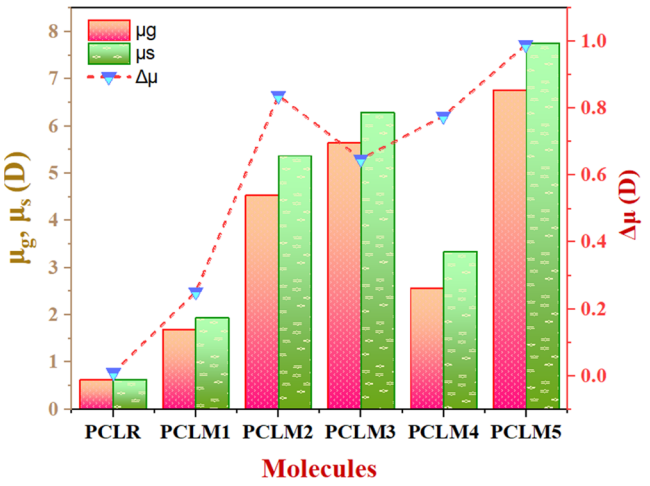

Figure 9. Graphical description of dipole moments at the ground (μ_g) and excited (μ_s) states and their difference ($\Delta\mu$) for **PCLR** and **PCLM1−PCLM5**.

Table 6. Role of the Core, Spacer, and Acceptor in Escalating the HOMO/LUMO Energy Levels of PCLR and PCLM1−PCLM5

molecules	HOMO = H LUMO = L	core (eV)	spacer (eV)	acceptor (eV)
PCLR	H	23.6	36.3	40.2
	L	30.1	26.2	43.7
PCLM1	H	8.1	27.9	64
	L	31.7	25.0	43.3
PCLM2	H	11.3	34.7	54.0
	L	34.5	23.9	41.5
PCLM3	H	23.6	36.3	40.2
	L	30.1	26.2	43.7
PCLM4	H	10.2	31.6	58.2
	L	29.0	24.3	46.7
PCLM5	H	5.9	9.1	85.0
	L	36.9	15.6	47.5

inferior E_b values compared with that of **PCLR**, which indicates the presence of weak Coulombic interactions and easy separation of the bound hole−electron pairs.

The E_b values of the reference **PCLR** and the newly fabricated molecules (**PCLM1−PCLM5**) in $CHCl_3$ were 0.4, 0.36, 0.39, 0.38, 0.37, and 0.34 eV, respectively, as indicated in Table 7. Among all molecules, **PCLM1** showed the smallest E_b value, which implied its efficient charge-generation properties.

Transition density matrix (TDM) analysis is another effective method for investigating electronic excitation processes in real time (including the creation and dispersion of excitons, recombination, and separation of charges).[35] As a result of excitation measurements, the TDM may be used to investigate and understand the quantum geometry. The interaction between acceptor and donor moieties in the excited state is shown by TDM plots.[36] The TDM graphs of the reference **PCLR** and the newly constructed molecules (**PCLM1−PCLM5**) are demonstrated in Figure 12. For the TDM analysis, all the molecules were sectioned into three fragments, namely, the donor (**D**), π-spacer (**B**), and acceptor (**A**) moieties. In the TDM plots, the number of atoms partaking are represented by lower abscissa and ordinates on the left side, whereas the right ordinates indicate the flow of electron density.

Since hydrogen atoms have minimal influence on the transitions, they have been ignored in the TDM analysis.[37] It can be understood from the TDM graph analysis of **PCLR, PCLM1, PCLM3**, and **PCLM4** that the electron density is shifted from **D** to **A** via **B** of the DPP acceptor uniformly. The bright portion moving diagonally in the TDM graph shows the electron density. The examination of the TDM graphs of **PCLM2** and **PCLM5** showed that the molecule has a uniform diagonal electron density as well as off-diagonal charge transfer from **D** to **A** moieties. The brighter portion is more concentrated on **A** moieties, indicating the excellent charge transfer from **D** to **A** via π-conjugation. Hence, it is summarized that the newly fabricated molecules exhibit efficient charge-transmission and charge-dissociation properties.

3.7. Reorganization Energy (RE). Reorganization energy (RE) is an excellent analytical scheme for designing efficient OSCs and assessing the operating efficiency of OSCs. Electron and hole mobilities in a molecule during excitation are described by this energy.[38] Electrons and holes must be separated as they have different charges. The charge transferability shows an inverse relation with RE. When a molecule's charge mobility is low, it migrates toward the respective electrode readily. The electron and hole mobilities are statistically determined by eqs 1 and 2. The results of RE in terms of electron and hole mobilities of the reference **PCLR** and the five newly fabricated molecules (**PCLM1−PCLM5**) are reviewed in Table 8 and a pictorial representation is given in Figure 13.

After a careful evaluation, it is noted that the newly engineered molecules **PCLM1** (0.00428 eV), **PCLM2** (0.00292 eV), **PCLM3** (0.00516 eV), and **PCLM5** (0.00367 eV) have the least values of electron RE (λ_e) as compared with the reference **PCLR** (0.00552 eV), hence offering a better electron mobility rate. Also, all of our newly designed molecules have low values of hole RE (λ_h) compared with the reference **PCLR**, making them suitable candidates for hole-transport materials. The decreasing order of λ_h is **PCLR > PCLM4 > PCLM2 > PCLM3 > PCLM2 > PCLM1**.

3.8. Electrostatic Potential (ESP) Analysis. ESP is also crucial in predicting the relationship between the molecular structure, molecular interaction, and photophysical properties of molecules.[39] The ESP simulations performed at the selected functional determines the regions of nucleophiles and electrophiles in the researched molecule. The green color in ESP diagrams denotes the electrically neutral region, the red color shows the electrophilic regions having an abundance of electrons, and finally the blue color is concentrated on the nucleophilic regions where there is a positive electrostatic potential and lack of electrons.[38,40]

ESP analysis of all doped complexes (**PCLM1−PCLM5**) along with **PCLR** was performed theoretically at the MPW1PW91/6-31G** functional level. Figure 14 shows colored ESP maps of the **PCLR** and the freshly designed molecules (**PCLM1−PCLM5**). ESP surfaces of all of these molecules illustrate that the red color (negative potential) is concentrated on the acceptor regions of molecules, making them more electrophilic. The region where the donor exists in each molecular framework possesses a blue color (positive potential) and behaves as a nucleophile.

3.9. Open-Circuit Voltage (V_{OC}). Another credible approach to evaluate the OSC's operating efficiency is the open-circuit voltage (V_{OC}). V_{OC} is basically that maximum amount of current, which is produced when the externally applied voltage is zero.[41] Variables such as the donor's HOMO

https://doi.org/10.1021/acsomega.2c00001
ACS Omega 2022, 7, 20528−20541

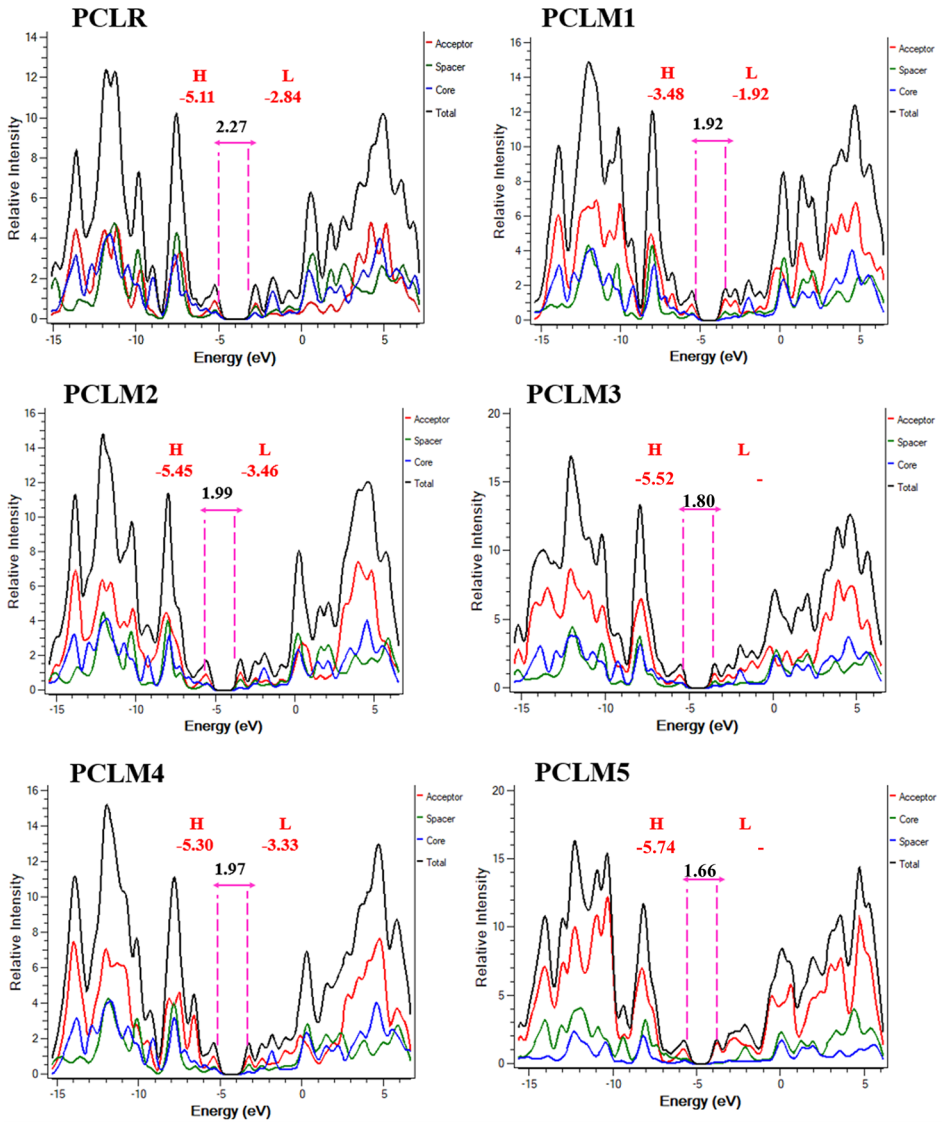

Figure 10. DOS graphs of the reference (**PCLR**) and designed chromophores (**PCLM1−PCLM5**).

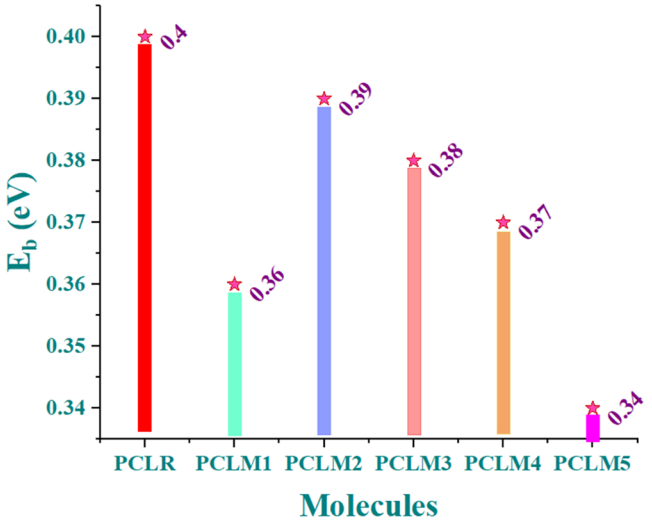

Figure 11. Graphical illustration of computed binding energy (E_b) values of **PCLR** and **PCLM1−PCLM5**.

Table 7. Theoretically Computed Values of Binding Energy (E_b) from the Energy Gap ($E_{L\text{-}H}$) between the FMOs and the Excitation Energy (E_{opt}) of PCLR and PCLM1−PCLM5

molecules	$E_{L\text{-}H}$ (eV)	E_{opt} (eV)	E_b (eV)
PCLR	2.27	1.87	0.40
PCLM1	1.92	1.56	0.36
PCLM2	1.99	1.60	0.39
PCLM3	1.80	1.42	0.38
PCLM4	1.97	1.60	0.37
PCLM5	1.66	1.32	0.34

and acceptor's LUMO are scaled up. V_{OC} is estimated with the selected MPW1PW91 functional. The mathematical expression used for computing V_{OC} is expressed by eq 5.

$$V_{OC} = \frac{1}{e}(|E^{D}_{HOMO}| - |E^{A}_{LUMO}|) - 0.3 \quad (5)$$

Here, V_{OC} is open-circuit voltage (V_{OC}), e is the charge of the molecules in this study, and 0.3 is the empirical factor.

The designed chromophores (**PCLM1−PCLM5**) act as promising donors, and so their HOMOs were cross-examined

https://doi.org/10.1021/acsomega.2c00001
ACS Omega 2022, 7, 20528−20541

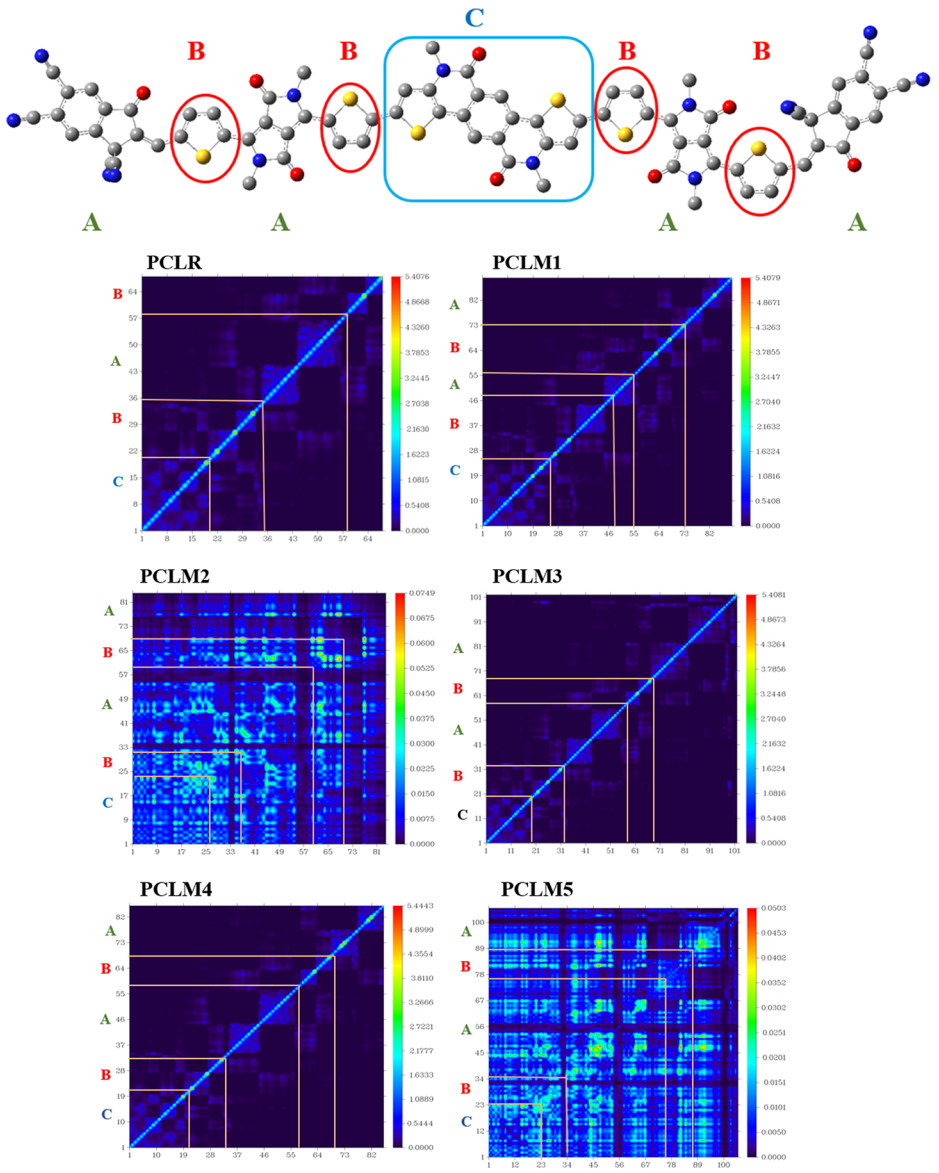

Figure 12. TDM plots of the reference (**PCLR**) and the designed chromophores (**PCLM1−PCLM5**).

Table 8. Calculated Hole (λ_h) and Electron Mobilities (λ_e) of PCLR and PCLM1−PCLM5

molecules	λ_e (eV)	λ_h (eV)
PCLR	0.00552	0.00623
PCLM1	0.00428	0.00497
PCLM2	0.00292	0.00550
PCLM3	0.00516	0.00523
PCLM4	0.00561	0.00561
PCLM5	0.00367	0.00497

with the LUMO of $PC_{61}BM$. **$PC_{61}BM$** is a widely used acceptor. In the present quantum chemical investigation, **$PC_{61}BM$** is geometrically optimized at the MPW1PW91 functional level. To obtain a higher V_{OC} value, it should be taken into account that the donor's HOMO has to be at a higher level and the LUMO of acceptor at a low level of energy. Figure 15 depicts the V_{OC} values of the reference **PCLR** and the newly investigated chromophores (**PCLM1−PCLM5**) along with the acceptor **$PC_{61}BM$**.

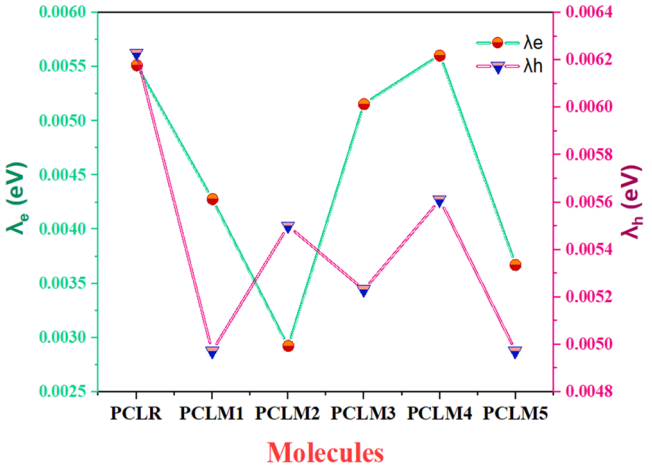

Figure 13. Plot of hole (λ_h) and electron (λ_e) mobilities for **PCLR** and **PCLM1−PCLM5**.

https://doi.org/10.1021/acsomega.2c00001
ACS Omega 2022, 7, 20528−20541

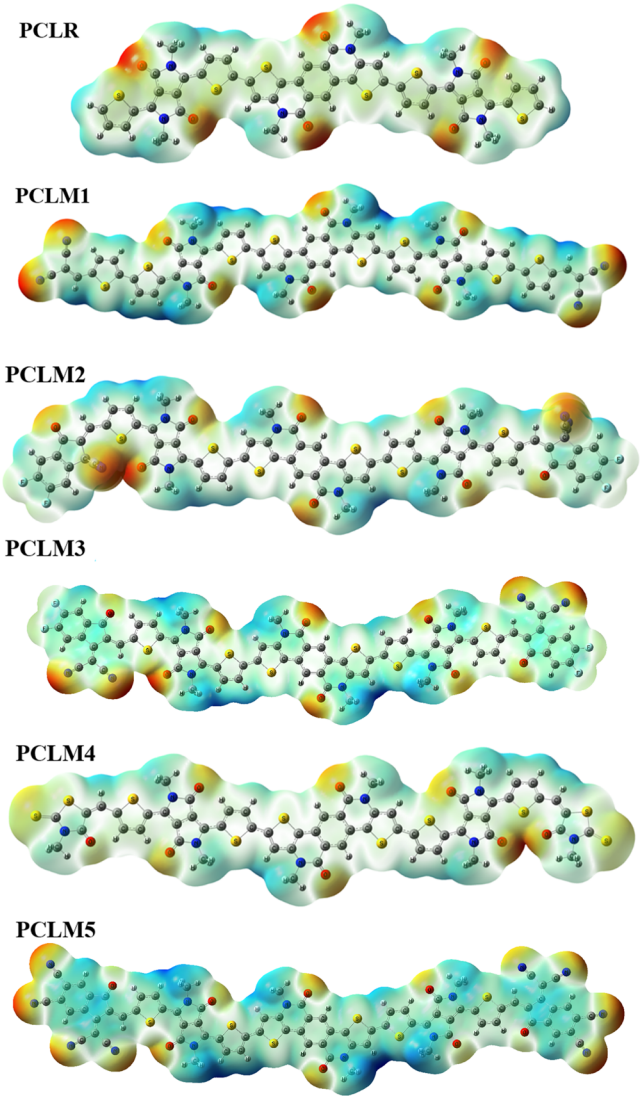

Figure 14. ESP depiction of **PCLR** and **PCLM1−PCLM5**.

The V_{OC} value of the reference **PCLR** computed when blended with $PC_{61}BM$ was 1.11 eV. V_{OC} values of the newly fabricated chromophores (**PCLM1−PCLM5**) were 1.40, 1.45, 1.52, 1.30, and 1.74 eV, respectively. All of our newly constructed chromophores showed a pronounced shift in V_{OC} values when compared with **PCLR**. It can be predicted that all designed chromophores can contribute to improving the device performance owing to their better charge-conduction properties.

3.10. Fill Factor (FF) and Power Conversion Efficiency (PCE). The fill factor (FF) is one the most prominent determining element and integral parameter to calculate the PCE of OSCs. V_{OC} of the donor−acceptor interface has a significant influence on FF.[42] FF is mathematically computed using eq 6 expressed below:

$$FF = \frac{\frac{eV_{oc}}{K_B T} - \ln\left(\frac{eV_{oc}}{K_B T} + 0.72\right)}{\frac{eV_{oc}}{K_B T} + 1} \quad (6)$$

In this equation, $\frac{eV_{oc}}{K_B T}$ illustrates the normalized open-circuit voltage, e represent the fixed charge on each molecule (taken to be 1), K_B represents the Boltzmann constant, and T is the temperature in Kelvin. Calculated values for normalized V_{OC}, along with the FF, are given in Table 9. All newly designed chromophores (**PCLM1−PCLM5**) have revealed a higher value of FF than **PCLR**. The greater FF supports the efficacy of the newly designed structures for future high-potential solar devices.

Table 9. Computed Open-Circuit Voltage (V_{OC}), Normalized V_{OC}, Fill Factor (FF), and Power Conversion Efficiency (PCE) of all Studied Molecules (PCLR and PCLM1−PCLM5)

molecules	V_{OC} (eV)	normalized V_{OC} (eV)	FF	J_{sc} (mA cm^{-2}) (this assumed short circuit current was taken from reference paper)	PCE (%)
PCLR	1.11	43.224	0.8918	9.7	9.603
PCLM1	1.40	54.517	0.9097	9.7	12.35
PCLM2	1.45	56.464	0.9122	9.7	12.83
PCLM3	1.52	58.796	0.9149	9.7	13.49
PCLM4	1.30	50.623	0.9043	9.7	11.40
PCLM5	1.74	67.306	0.9235	9.7	15.59

The PCE value for a device helps one to predict its working accuracy and mechanism.[43] PCE relies on a few essential parameters, which are given in eq 7.

$$PCE = \frac{J_{sc}\, V_{oc} FF}{P_{in}} \quad (7)$$

In the above equation, P_{in} represents an empirical constant, which depicts the power of the incident radiation that strikes the surface of the cell. The remaining quantities, i.e., the short-circuit current (J_{sc}), V_{OC}, and FF, have an association with the PCE value. Computed PCE values of the studied chromophores are displayed in Table 9. An incremental effect is observed in the

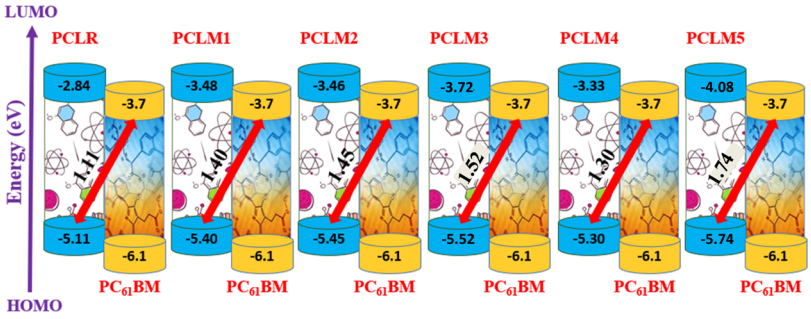

Figure 15. Pictorial view of the open-circuit voltage (V_{OC}) of **PCLR** and all of the newly modeled chromophores (**PCLM1−PCLM5**).

https://doi.org/10.1021/acsomega.2c00001
ACS Omega 2022, 7, 20528−20541

PCE for all novelly designed molecules (**PCLM1−PCLM5**) in comparison with that of the reference molecule (**PCLR**, 9.603%).

4. CONCLUSIONS

To summarize the above results, five pentacyclic aromatic bislactam (**PCL**)-based small donor groups (**PCLM1−PCLM5**) were fabricated from the reference **PCLR**, and their optoelectronic properties were computed at the MPW1PW91/6-31G** level. The newly modeled chromophores (**PCLM1−PCLM5**) showed satisfactory and competent results from DFT and TD-DFT computations. All of our novel molecules exhibited a lower bandgap and a red-shifted λ_{max} compared with the reference **PCLR** due to their strong electron-pulling moieties. The newly designed chromophores **PCLM1** (**796 nm**), **PCLM2** (**775 nm**), **PCLM3** (**874 nm**), **PCLM4** (**777 nm**), and **PCLM5** (**959 nm**) displayed higher λ_{max} values than **PCLR** (**662 nm**) in a $CHCl_3$ solvent. The bandgaps of the devised molecules ranged from 1.66 to 1.99 eV, whereas that of **PCLR** was **2.27 eV**. Likewise, the binding energies of all molecules were reduced in comparison with that of **PCLR**. An increase in the dipole moment was seen for all molecules in the $CHCl_3$ solvent, as opposed to the gaseous phase, resulting in better solubility and charge recombination. Moreover, the minimal λ_e and λ_h values of all of these newly designed molecules represent their higher electron and hole mobility rates, sequentially. The evaluation of the FMOs disclosed the uniform dispersal of charge density in the HOMOs and LUMOs of the newly fabricated molecules. According to a TDM analysis, the bound electron−hole pairs of the newly designed donor molecules (**PCLM1−PCLM5**) can be easily dissociated into electrons and holes because of their lower interaction coefficient. Furthermore, when scaled with a **$PC_{61}BM$** acceptor, all of the newly proposed molecules exhibited greater V_{OC} values than **PCLR**, which implies that these donor molecules play an important role in increasing the operational efficiency. Therefore, in this assay, highly productive PCE values in the range of 11.4−15.59% were estimated for the novelly designed molecules based on the normalized Voc and FF, which predict an increase in their photovoltaic efficiency compared with that of the reference **PCLR** (**9.603%**). It has been summarized that structural modification is an effective strategy to construct new organic materials for designing OSCs in the near future.

■ ASSOCIATED CONTENT

Supporting Information

The Supporting Information is available free of charge at https://pubs.acs.org/doi/10.1021/acsomega.2c00001.

Cartesian coordinates of internally optimized geometries of all molecules (reference **PCLR**, **PCLM1**, **PCLM2**, **PCLM3**, **PCLM4**, and **PCLM5**) along the *X*, *Y*, and *Z* axes at the MPW1PW91/6-31G (d, p) level of the density functional theory (PDF)

■ AUTHOR INFORMATION

Corresponding Authors

Rasheed Ahmad Khera − *Department of Chemistry, University of Agriculture, Faisalabad 38000, Pakistan;* orcid.org/0000-0002-5513-8096; Email: rasheedahmadkhera@yahoo.com, rasheed.ahmad.khera@uaf.edu.pk

Javed Iqbal − *Department of Chemistry, University of Agriculture, Faisalabad 38000, Pakistan; Punjab Bio-energy Institute, University of Agriculture, Faisalabad 38000, Pakistan;* orcid.org/0000-0003-0598-8401; Email: javedkhattak79@gmail.com, Javed.iqbal@uaf.edu.pk

Authors

Mahnoor Qaisar − *Department of Chemistry, University of Agriculture, Faisalabad 38000, Pakistan*

Saba Zahid − *Department of Chemistry, University of Agriculture, Faisalabad 38000, Pakistan;* orcid.org/0000-0002-9835-6317

Yaser A. El-Badry − *Chemistry Department, Faculty of Science, Taif University, khurma, Taif 21944, Saudi Arabia*

Muhammad Umar Saeed − *Department of Chemistry, University of Agriculture, Faisalabad 38000, Pakistan*

Rana Farhat Mehmood − *Department of Chemistry, Division of Science and Technology, University of Education, Lahore 54770, Pakistan*

Complete contact information is available at: https://pubs.acs.org/10.1021/acsomega.2c00001

Notes

The authors declare no competing financial interest.

■ ACKNOWLEDGMENTS

The authors acknowledge the financial and technical support from the Punjab Bio-energy Institute (PBI), University of Agriculture, Faisalabad (UAF), Pakistan. The authors gratefully acknowledge the financial support provided from the Taif University Researchers Supporting Project number TURSP-2020/ 106, Taif University, Taif, Saudi Arabia. We are also thankful to Dr. Khurshid Ayub, Department of Chemistry, COMSATS University Islamabad, Abbottabad Campus, for additional resources.

■ REFERENCES

(1) Rahman, M. M.; Velayutham, E. Renewable and non-renewable energy consumption-economic growth nexus: new evidence from South Asia. *Renewable Energy* **2020**, *147*, 399−408.

(2) (a) Sun, J.; Zhang, Z.; Yin, X.; Zhou, J.; Yang, L.; Geng, R.; Zhang, F.; Zhu, R.; Yu, J.; Tang, W. High performance non-fullerene polymer solar cells based on PTB7-Th as the electron donor with 10.42% efficiency. *J. Mater. Chem. A* **2018**, *6*, 2549−2554. (b) Gong, J.; Sumathy, K.; Qiao, Q.; Zhou, Z. Review on dye-sensitized solar cells (DSSCs): Advanced techniques and research trends. *Renewable Sustainable Energy Rev.* **2017**, *68*, 234−246.

(3) Yao, J.; Zheng, X.; Xu, J.; Wu, K. In *Cross-Technology Communication through Symbol-Level Energy Modulation for Commercial Wireless Networks 2020*, IEEE International Conference on Pervasive Computing and Communications (PerCom); IEEE, 2020; pp 1−10.

(4) (a) Mujahid, M.; Chen, C.; Hu, W.; Wang, Z.-K.; Duan, Y. Progress of high-throughput and low-cost flexible perovskite solar cells. *Sol. RRL* **2020**, *4*, No. 1900556. (b) Iqbal, J.; Enevold, J.; Larsen, C.; Wang, J.; Revoju, S.; Barzegar, H. R.; Wågberg, T.; Eliasson, B.; Edman, L. An arylene-vinylene based donor-acceptor-donor small molecule for the donor compound in high-voltage organic solar cells. *Sol. Energy Mater. Sol. Cells* **2016**, *155*, 348−355.

(5) Riede, M.; Spoltore, D.; Leo, K. Organic solar cells—the path to commercial success. *Adv. Energy Mater.* **2021**, *11*, No. 2002653.

(6) (a) Zhang, G.; Zhao, J.; Chow, P. C.; Jiang, K.; Zhang, J.; Zhu, Z.; Zhang, J.; Huang, F.; Yan, H. Nonfullerene acceptor molecules for bulk heterojunction organic solar cells. *Chem. Rev.* **2018**, *118*, 3447−3507. (b) Rafique, S.; Abdullah, S. M.; Sulaiman, K.; Iwamoto, M. Fundamentals of bulk heterojunction organic solar cells: An overview

of stability/degradation issues and strategies for improvement. *Renewable Sustainable Energy Rev.* **2018**, *84*, 43−53.
(7) Schlachter, A.; Marineau-Plante, G.; Harvey, P. D.; Agrawal, A.; Sharma, G. D. Efficient ternary bulk heterojunction organic solar cells using a low-cost nonfullerene acceptor. *J. Mater. Chem. C* **2022**, *10*, 4372−4382.
(8) (a) Liu, G.; Jia, J.; Zhang, K.; Jia, Xe.; Yin, Q.; Zhong, W.; Li, L.; Huang, F.; Cao, Y. 15% efficiency tandem organic solar cell based on a novel highly efficient wide-bandgap nonfullerene acceptor with low energy loss. *Adv. Energy Mater.* **2019**, *9*, No. 1803657. (b) Ostroverkhova, O. *Handbook of organic materials for optical and (opto) electronic devices: properties and applications*, Elsevier, 2013.
(9) (a) Nielsen, C. B.; Holliday, S.; Chen, H.-Y.; Cryer, S. J.; McCulloch, I. Non-fullerene electron acceptors for use in organic solar cells. *Acc. Chem. Res.* **2015**, *48*, 2803−2812. (b) McAfee, S. M.; Topple, J. M.; Hill, I. G.; Welch, G. C. Key components to the recent performance increases of solution processed non-fullerene small molecule acceptors. *J. Mater. Chem. A* **2015**, *3*, 16393−16408. (c) Lin, Y.; Zhan, X. Oligomer molecules for efficient organic photovoltaics. *Acc. Chem. Res.* **2016**, *49*, 175−183.
(10) (a) Cui, Y.; Yao, H.; Zhang, J.; Xian, K.; Zhang, T.; Hong, L.; Wang, Y.; Xu, Y.; Ma, K.; An, C.; et al. Single-junction organic photovoltaic cells with approaching 18% efficiency. *Adv. Mater.* **2020**, *32*, No. 1908205. (b) Liu, T.; Ma, R.; Luo, Z.; Guo, Y.; Zhang, G.; Xiao, Y.; Yang, T.; Chen, Y.; Li, G.; Yi, Y.; et al. Concurrent improvement in J sc and V oc in high-efficiency ternary organic solar cells enabled by a red-absorbing small-molecule acceptor with a high LUMO level. *Energy Environ. Sci.* **2020**, *13*, 2115−2123. (c) Ans, M.; Paramasivam, M.; Ayub, K.; Ludwig, R.; Zahid, M.; Xiao, X.; Iqbal, J. Designing alkoxy-induced based high performance near infrared sensitive small molecule acceptors for organic solar cells. *J. Mol. Liq.* **2020**, *305*, No. 112829. (d) Ma, R.; Liu, T.; Luo, Z.; Gao, K.; Chen, K.; Zhang, G.; Gao, W.; Xiao, Y.; Lau, T.-K.; Fan, Q.; et al. Adding a third component with reduced miscibility and higher LUMO level enables efficient ternary organic solar cells. *ACS Energy Lett.* **2020**, *5*, 2711−2720. (e) Wang, X.; Chen, H.; Ran, A.-R.; Luo, L.; Chan, P. P.; Tham, C. C.; Chang, R. T.; Mannil, S. S.; Cheung, C. Y.; Heng, P.-A. Towards multi-center glaucoma OCT image screening with semi-supervised joint structure and function multi-task learning. *Med. Image Anal.* **2020**, *63*, No. 101695.
(11) Zhao, W.; Li, S.; Yao, H.; Zhang, S.; Zhang, Y.; Yang, B.; Hou, J. Molecular optimization enables over 13% efficiency in organic solar cells. *J. Am. Chem. Soc.* **2017**, *139*, 7148−7151.
(12) (a) Cao, Y.; Guo, Z.-H.; Chen, Z.-Y.; Yuan, J.-S.; Dou, J.-H.; Zheng, Y.-Q.; Wang, J.-Y.; Pei, J. Pentacyclic aromatic bislactam-based conjugated polymers: constructed by Beckmann rearrangement and application in organic field-effect transistor. *Polym. Chem.* **2014**, *5*, 5369−5374. (b) Truong, N. T. T.; Nguyen, L. T.; Mai, H. L. T.; Doan, B. K.; Tran, D. H.; Truong, K. T.; Nguyen, V. Q.; Nguyen, L.-T. T.; Hoang, M. H.; Van Pham, T.; et al. Phenothiazine derivatives, diketopyrrolopyrrole-based conjugated polymers: synthesis, optical and organic field effect transistor properties. *J. Polym. Res.* **2020**, *27*, No. 223.
(13) (a) Chen, Z.; Huang, J.; Zhang, W.; Zhou, Y.; Wei, X.; Wei, J.; Zheng, Y.; Wang, L.; Yu, G. Tunable charge-transport polarity in thienothiophene−bisoxoindolinylidene-benzodifurandione copolymers for high-performance field-effect transistors. *J. Mater. Chem. C* **2022**, *10*, 2671−2680. (b) Tam, T. L. D.; Handoko, A. D.; Lin, T. T.; Xu, J. Electron n-doping of a highly electron-deficient chlorinated benzodifurandione-based oligophenylene vinylene polymer using benzyl viologen radical cations. *Mater. Chem. Front.* **2021**, *5*, 6182−6191.
(14) Zhou, J.; Zuo, Y.; Wan, X.; Long, G.; Zhang, Q.; Ni, W.; Liu, Y.; Li, Z.; He, G.; Li, C.; et al. Solution-processed and high-performance organic solar cells using small molecules with a benzodithiophene unit. *J. Am. Chem. Soc.* **2013**, *135*, 8484−8487.
(15) (a) Hong, W.; Sun, B.; Aziz, H.; Park, W.-T.; Noh, Y.-Y.; Li, Y. A conjugated polyazine containing diketopyrrolopyrrole for ambipolar organic thin film transistors. *Chem. Commun.* **2012**, *48*, 8413−8415. (b) Sonar, P.; Zhuo, J.-M.; Zhao, L.-H.; Lim, K.-M.; Chen, J.; Rondinone, A. J.; Singh, S. P.; Chua, L.-L.; Ho, P. K.; Dodabalapur, A. Furan substituted diketopyrrolopyrrole and thienylenevinylene based low band gap copolymer for high mobility organic thin film transistors. *J. Mater. Chem.* **2012**, *22*, 17284−17292.
(16) Feng, G.; Xu, Y.; Zhang, J.; Wang, Z.; Zhou, Y.; Li, Y.; Wei, Z.; Li, C.; Li, W. All-small-molecule organic solar cells based on an electron donor incorporating binary electron-deficient units. *J. Mater. Chem. A* **2016**, *4*, 6056−6063.
(17) Adamo, C.; Barone, V. Exchange functionals with improved long-range behavior and adiabatic connection methods without adjustable parameters: The m PW and m PW1PW models. *J. Chem. Phys.* **1998**, *108*, 664−675.
(18) Civalleri, B.; Zicovich-Wilson, C. M.; Valenzano, L.; Ugliengo, P. B3LYP augmented with an empirical dispersion term (B3LYP-D*) as applied to molecular crystals. *CrystEngComm* **2008**, *10*, 405−410.
(19) Chai, J.-D.; Head-Gordon, M. Long-range corrected hybrid density functionals with damped atom−atom dispersion corrections. *Phys. Chem. Chem. Phys.* **2008**, *10*, 6615−6620.
(20) Yanai, T.; Tew, D. P.; Handy, N. C. A new hybrid exchange−correlation functional using the Coulomb-attenuating method (CAM-B3LYP). *Chem. Phys. Lett.* **2004**, *393*, 51−57.
(21) Bjorgaard, J. A.; Velizhanin, K. A.; Tretiak, S. Solvent effects in time-dependent self-consistent field methods. II. Variational formulations and analytical gradients. *J. Chem. Phys.* **2015**, *143*, No. 054305.
(22) Gorelsky, S. *SWizard program*; University of Ottawa: Ottawa, Canada, 2010.
(23) Deschenes, L. A.; David, A.Vanden BoutUniversity of Texas, *A. Origin 6.0: Scientific Data Analysis and Graphing Software Origin Lab Corporation (formerly Microcal Software, Inc.)*, ACS Publications, Web site: www.originlab.com, Commercial price: 595.Academicprice: 446, 2000.
(24) Tenderholt, A. L.; Szilagyi, R. K.; Holm, R. H.; Hodgson, K. O.; Hedman, B.; Solomon, E. I. Electronic Control of the "Bailar Twist" in Formally d0-d2 Molybdenum Tris (dithiolene) Complexes: A Sulfur K-edge X-ray Absorption Spectroscopy and Density Functional Theory Study. *Inorg. Chem.* **2008**, *47*, 6382−6392.
(25) Lu, T.; Chen, F. Multiwfn: a multifunctional wavefunction analyzer. *J. Comput. Chem.* **2012**, *33*, 580−592.
(26) Shehzad, R. A.; Muhammad, S.; Iqbal, J.; Al-Sehemi, A. G.; Yaseen, M.; Aloui, Z.; Khalid, M. Exploring the optoelectronic and third-order nonlinear optical susceptibility of cross-shaped molecules: insights from molecule to material level. *J. Mol. Model.* **2021**, *27*, No. 12.
(27) Rasool, A.; Zahid, S.; Shehzad, R. A.; Akhter, M. S.; Iqbal, J. Designing of benzodithiophene (BDT) based non-fullerene small molecules with favorable optoelectronic properties for proficient organic solar cells. *Comput. Theor. Chem.* **2021**, *1203*, No. 113359.
(28) (a) Jilani, F.; Iqbal, J.; Shahid, I.; Yaseen, M.; Mahr, M. S.; Khalid, M.; Ayub, K. Rational design of naphthalimide based small molecules non-fullerene acceptors for organic solar cells. *Comput. Theor. Chem.* **2020**, *1187*, No. 112916. (b) Asif, T.; Khera, R. A.; Naveed, A.; Salim, M.; Iqbal, J. Tuning the optoelectronic properties of naphthodithiophene (NDT) for designing of ADA type photovoltaic materials. *Optik* **2021**, *247*, No. 167892.
(29) Zahid, S.; Rasool, A.; Shehzad, R. A.; Bhatti, I. A.; Iqbal, J. Tuning the optoelectronic properties of triphenylamine (TPA) based small molecules by modifying central core for photovoltaic applications. *J. Mol. Model.* **2021**, *27*, No. 237.
(30) Khan, M. U.; Khalid, M.; Ibrahim, M.; Braga, A. A. C.; Safdar, M.; Al-Saadi, A. A.; Janjua, M. R. S. A. First theoretical framework of triphenylamine−dicyanovinylene-based nonlinear optical dyes: structural modification of π-linkers. *J. Phys. Chem. C* **2018**, *122*, 4009−4018.
(31) Zahid, S.; Rasool, A.; Ayub, A. R.; Ayub, K.; Iqbal, J.; Al-Buriahi, M. S.; Alwadai, N.; Somaily, H. H. Silver cluster doped graphyne (GY) with outstanding non-linear optical properties. *RSC Adv.* **2022**, *12*, 5466−5482.
(32) (a) Fonseca Guerra, C.; Handgraaf, J. W.; Baerends, E. J.; Bickelhaupt, F. M. Voronoi deformation density (VDD) charges: Assessment of the Mulliken, Bader, Hirshfeld, Weinhold, and VDD

https://doi.org/10.1021/acsomega.2c00001
ACS Omega 2022, 7, 20528−20541

methods for charge analysis. *J. Comput. Chem.* **2004**, *25*, 189−210. (b) Naeem, M.; Jabeen, S.; Khera, R. A.; Mubashar, U.; Iqbal, J. Tuning of optoelectronic properties of triphenylamines-based donor materials for organic solar cells. *J. Theor. Comput. Chem.* **2019**, *18*, No. 1950036.
(33) Clarke, T. M.; Durrant, J. R. Charge photogeneration in organic solar cells. *Chem. Rev.* **2010**, *110*, 6736−6767.
(34) Köse, M. E. Evaluation of acceptor strength in thiophene coupled donor−acceptor chromophores for optimal design of organic photovoltaic materials. *J. Phys. Chem. A* **2012**, *116*, 12503−12509.
(35) Naveed, A.; Khera, R. A.; Azeem, U.; Zubair, I.; Farhat, A.; Ayub, A. R.; Iqbal, J. Tuning the optoelectronic properties of benzodithiophene based donor materials and their photovoltaic applications. *Mater. Sci. Semicond. Process.* **2022**, *137*, No. 106150.
(36) Farhat, A.; Khera, R. A.; Iqbal, S.; Iqbal, J. Tuning the optoelectronic properties of Subphthalocyanine (SubPc) derivatives for photovoltaic applications. *Opt. Mater.* **2020**, *107*, No. 110154.
(37) Sabir, S.; Khera, R. A.; Jabeen, S.; Shafiq, Z.; Musawwir, A.; Iqbal, J. Tuning the optoelectronic properties of Benzo Thiophene (BT-CIC) based non-fullerene acceptor organic solar cell. *J. Theor. Comput. Chem.* **2020**, *19*, No. 2050003.
(38) Zahid, S.; Rasool, A.; Ans, M.; Yaseen, M.; Iqbal, J. Quantum Chemical Approach of Donor− π−Acceptor Based Arylborane−Arylamine Macrocycles with Outstanding Photovoltaic Properties Toward High-Performance Organic Solar Cells. *Energy Fuels* **2021**, *35*, 15018−15032.
(39) Drissi, M.; Benhalima, N.; Megrouss, Y.; Rachida, R.; Chouaih, A.; Hamzaoui, F. Theoretical and experimental electrostatic potential around the m-nitrophenol molecule. *Molecules* **2015**, *20*, 4042−4054.
(40) Zahid, S.; Rasool, A.; Ans, M.; Akhter, M. S.; Iqbal, J.; Al-Buriahi, M.; Alomairy, S.; Alrowaili, Z. Environmentally compatible and highly improved hole transport materials (HTMs) based on benzotrithiophene (BTT) skeleton for perovskite as well as narrow bandgap donors for organic solar cells. *Sol. Energy* **2022**, *231*, 793−808.
(41) Rasool, A.; Zahid, S.; Ans, M.; Muhammad, S.; Ayub, K.; Iqbal, J. Bithieno Thiophene-Based Small Molecules for Application as Donor Materials for Organic Solar Cells and Hole Transport Materials for Perovskite Solar Cells. *ACS Omega* **2022**, *7*, 844−862.
(42) (a) Yaqoob, U.; Ayub, A. R.; Rafiq, S.; Khalid, M.; El-Badry, Y. A.; El-Bahy, Z. M.; Iqbal, J. Structural, optical and photovoltaic properties of unfused Non-Fullerene acceptors for efficient solution processable organic solar cell (Estimated PCE greater than 12.4%): A DFT approach. *J. Mol. Liq.* **2021**, *341*, No. 117428. (b) Jao, M.-H.; Liao, H.-C.; Su, W.-F. Achieving a high fill factor for organic solar cells. *J. Mater. Chem. A* **2016**, *4*, 5784−5801.
(43) Chen, J. D.; Cui, C.; Li, Y. Q.; Zhou, L.; Ou, Q. D.; Li, C.; Li, Y.; Tang, J. X. Single-junction polymer solar cells exceeding 10% power conversion efficiency. *Adv. Mater.* **2015**, *27*, 1035−1041.

https://doi.org/10.1021/acsomega.2c00001
ACS Omega 2022, 7, 20528−20541